Materials Advances

ROYAL SOCIETY OF CHEMISTRY

REVIEW

View Article Online
View Journal | View Issue

Cite this: *Mater. Adv.*, 2024, 5, 51

A review on zirconium-based metal–organic frameworks: synthetic approaches and biomedical applications

Krishna Chattopadhyay, *[a] Manas Mandal *[b] and Dilip Kumar Maiti *[a]

Received 19th September 2023,
Accepted 20th November 2023

DOI: 10.1039/d3ma00735a

rsc.li/materials-advances

Since the last decade, metal–organic frameworks (MOFs) have received great attention from the materials scientist community owing to their excellent storage capacities, high surface area with tunable porous structures, functionalization-friendliness and biocompatible nature, which enable MOF-based materials to be suitable for biomedical applications. Zirconium-based MOFs (Zr-MOFs) are comparatively stable with low cytotoxicity and high drug-loading capacity. Therefore, Zr-MOFs and their composites have been thoroughly investigated for various bio-related applications such as drug delivery, anti-cancer activity, bio-sensing, and imaging. This review article demonstrates the recently developed synthetic routes for various surface-functionalized Zr-MOFs with their advantages and disadvantages. This review concisely summarizes some important Zr-based MOFs employed for biomedical applications such as drug delivery, immunoassay, antitumor activity, cytotoxicity activity, *etc.* Finally, a comparative analysis of the mode of action of the Zr-MOFs with varying organic linkers for biomedical applications is also provided to afford new directions for further research.

1. Introduction

Metal–organic frameworks (MOFs) are a category of crystalline nanoporous materials with self-assembling structures, consisting of inorganic metal clusters and flexible organic ligands. These organic ligands are connectors between the inorganic clusters within the framework, allowing for extensive customization possibilities. The impressive storage capabilities, coupled with a

[a] *Department of Chemistry, University of Calcutta, Kolkata 700009, India. E-mail: krishchem001@gmail.com, dkmchem@caluniv.ac.in*
[b] *Department of Chemistry, Sree Chaitanya College, Habra, WB 743268, India. E-mail: manasmandal26@gmail.com*

Krishna Chattopadhyay

Krishna Chattopadhyay is a Woman Scientist in the Department of Chemistry, University of Calcutta. She was previously a postdoctoral researcher at IACS, Kolkata. She received her PhD in Chemistry from IIT Kharagpur in 2017, her MSc in Chemistry from The University of Burdwan in 2012, and her BSc degree in Chemistry (Honours) from The University of Burdwan in 2010. Her research interest is focused on the design, synthesis, and fabrication of luminescent smart Nano-MOFs for the development of innovative pollution control, biocidal, nano-electronic device and energy storage applications.

Manas Mandal

Manas Mandal is an Assistant Professor of Department of Chemistry at the Sree Chaitanya College, Habra affiliated to the West Bengal State University. Earlier, he was a researcher in National University of Singapore (NUS). He received his PhD from the Jadavpur University in 2022. Before that he obtained MSc degree in Chemistry from IIT Kanpur and MTech in Materials Science & Engineering from IIT Kharagpur. His research interest lies in the field of nanomaterials for various applications, especially for electrochemical energy storage and water purification.

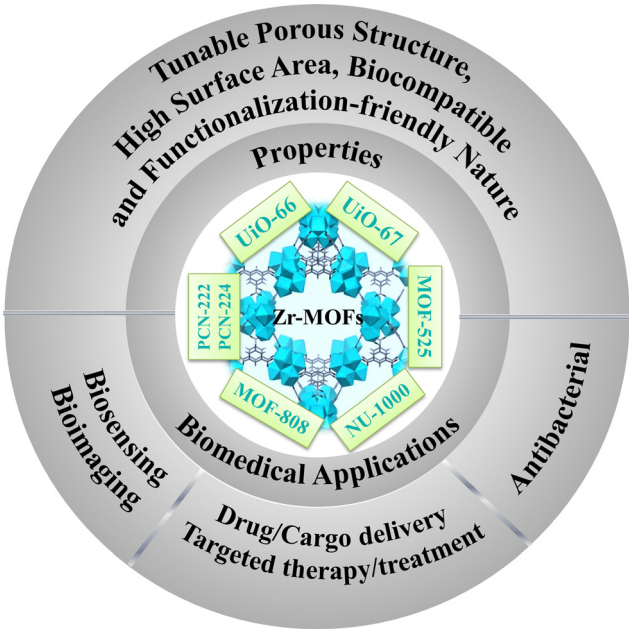

Scheme 1 Various properties and biomedical applications of Zr-MOFs.

tunable porous structure, high surface area, and the biocompatibility and functionalization-friendly nature of MOF materials make them well-suited for biomedical applications.[1–3] Furthermore, they play a significant role in the chemical industry, being extensively utilized for gas adsorption and separation, as well as in catalytic and sensing applications.[4,5] In the field of medicine, these versatile materials find diverse applications, ranging from biomedical imaging and biosensing to tumor therapy and targeted cancer therapy to bone therapy and repair.[6–8] The zirconium-based metal–organic frameworks (Zr-MOFs) stand out within the expansive category of MOFs, drawing significant attention due to their exceptional characteristics, including a substantial surface area, stability, adaptability for diverse applications, and the potential for post-modifications (Scheme 1).[9] Zirconium is extensively distributed in nature and present in all biological systems. The opulent content and little toxicity of Zr further support the development and application of Zr-MOFs.[10] The *in situ* or post-synthetic functionalization of the organic part improves the physiological properties of the MOFs. For example, it diminishes their cytotoxicity, enhances colloidal stability, and stimulates desirable degradation rate and efficient cellular intake. When considering MOFs for drug delivery purposes, it is crucial to prioritize traits such as high biocompatibility, biodegradability, and minimal cytotoxicity towards living cells. Among the myriad of MOFs synthesized over the past two decades, Zr-based MOFs are exceptionally biocompatible and possess the requisite properties for achieving effective drug delivery systems (DDS). Moreover, a range of hybrid materials can be produced using these MOFs, leading to exceptional candidates for drug delivery applications.

Lillerud *et al.* first reported the initial Zr MOFs in 2008.[11] The UiO series of MOFs UiO-66 and UiO-67, named after Universitetet i Oslo, consist of materials in which octahedral clusters $[Zr_6O_4(OH)_4(RCO_2)_{12}]$ are interconnected by linear dicarboxylate ligands, forming extended and highly porous networks represented by the general formula $[Zr_6O_4(OH)_4(L)_6]_n$. These Zr_6 clusters and their derivatives act as inorganic secondary building units (SBUs) in most Zr-based MOFs documented thus far. After that, with the progress in the field of biomedical application of MOFs, UiO-66, UiO-67, and other hybrid materials derived from them are extensively studied in the realm of biomedical applications. Numerous functionalized UiO-66 and UiO-67 are reported for drug delivery in treating tumor cells.[12–16]

Another Zr-porphyrin-based MOF family utilizes pristine TCPP (tetrakis(4-carboxyphenyl)porphyrin) ligands or M-TCPP complexes as linkers to connect the Zr_6 cluster nodes. This family of MOFs includes PCN-222, PCN-224, PCN-222(Fe), *etc.*[17] These Zr-porphyrinic MOFs are important in the field of NIR light or near-infrared-triggered photodynamic therapy (PDT) owing to the exceptional light harvesting properties of the TCPP linkers. These MOFs and their derivatives have been extensively examined for photoelectrochemical (PEC) immunoassay applications. The next group of Zr-MOFs, which are promising candidates for biomedical applications, is MOF-525, initially synthesized by Morris and colleagues.[18] This material is formed from a 12-connected Zr secondary building unit (SBU) denoted as $[Zr_6O_4(OH)_4]$ and a TCPP linker. The excellent fluorescence properties, combined with the ability to adsorb single-stranded nucleic acids make MOF-525 and related compounds potential candidates for the construction of fluorescent biosensors. There are numerous other Zr-MOFs like MOF-808, NU-1000, *etc.*, which have found potential applications in the biomedical field.

Despite the numerous review papers published on MOF materials, there is a scarcity of reviews focusing on the recent advancements in Zr-MOFs and their biomedical applications.[19–24] In this review, we have summarized different groups of Zr-based MOFs (Scheme 2) and their unique characteristics that are of benefit for biomedical applications. A comparative analysis of

Dilip Kumar Maiti

Dilip Kumar Maiti, FRSC, is a Professor in the Department of Chemistry, University of Calcutta. Prof. Maiti completed his BSc in chemistry in 1991 from Ramkrishna Mission Vidyamandir, University of Calcutta. Then he completed MSc from University of Calcutta in 1993. In the year of 1998, he received his PhD degree from Indian Institute of Chemical Biology, Jadavpur University. Then he joined Jadavpur University for post-doctoral studies. After that, he moved to the School of Medicine, Wayne State University, Detroit, USA as a post-doctoral fellow. His research focuses on design, synthesis, fabrication of smart organic nanomaterials and developing innovative applications.

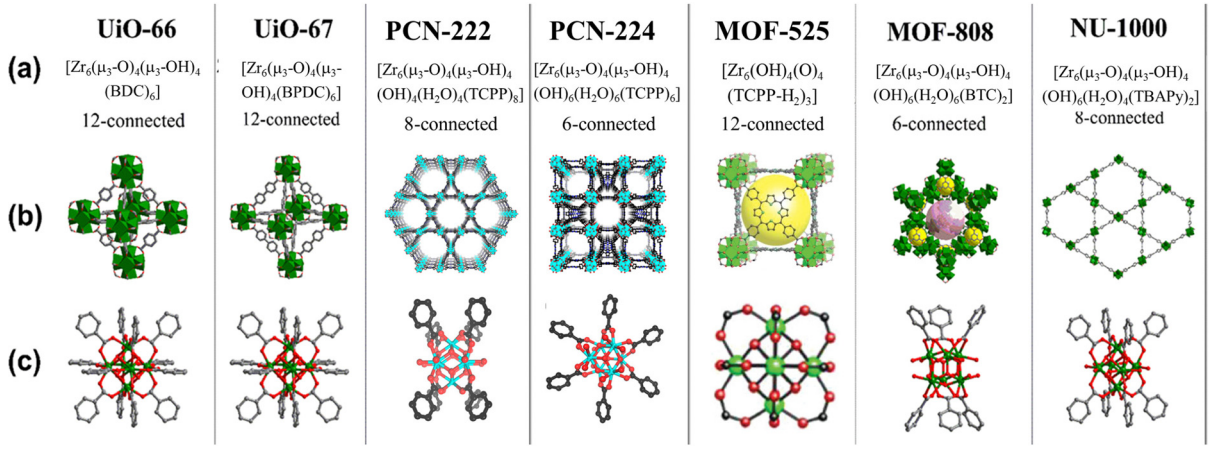

Scheme 2 Selected Zr-MOFs and their structures: (a) notations and formulations for the selected MOFs; (b) MOF structure; and (c) structures of the corresponding building units. Reproduced with permission from ref. 18,25,26. Copyright 2012, 2019 American Chemical Society.

various MOFs and their working strategies has been performed, which will benefit researchers for further research into biomedical applications of Zr-MOFs.

2. Synthetic strategies of Zr-MOFs

The choice of synthetic routes for MOFs can vary based on the desirable morphologies and properties. The conventional approaches for creating MOFs involve precipitation, solvo- or hydrothermal methods, which are commonly employed for crafting coordination networks. Additionally, there are more eco-friendly synthesis techniques, including ultrasound-assisted, ionothermal, sonochemical, microwave-assisted, and mechanochemical methods (Scheme 3). It is worth noting that numerous comprehensive reviews on MOF synthesis are available, so only a concise overview is presented here.[27]

2.1 Solvothermal method

There are several reports on pure and composites of UiO-66, which were synthesized using the solvothermal method.[28–30] Generally, dimethylformamide (DMF) is utilized to dissolve terephthalic acid and $ZrCl_4$, with respective quantities at 25 °C under vigorous stirring until a clear solution is obtained. Then $ZrOCl_2$ salt is added to the solution.[31] Subsequently, the solution is kept at 120 °C for 24 hours within a Teflon-lined hydrothermal autoclave, then gradually cooled to room temperature. Finally, the obtained nanoparticles are washed and placed in a vacuum drying oven at 120 °C to remove any remaining solvents. In this process, UiO-67 is also synthesized using a H_2bpydc organic linker instead of terephthalic acid.[32] NU-1000 and the porphyrinic Zr-MOFs like PCN-222, PCN-224 are also easily synthesized *via* a solvothermal method.[33–35]

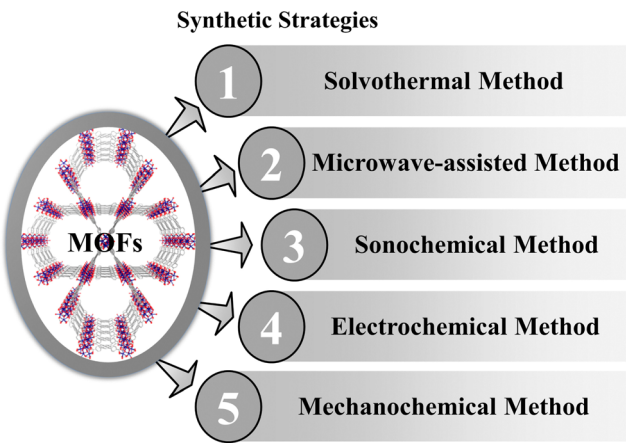

Scheme 3 Synthetic methods of MOFs.

2.2 Microwave-assisted synthesis

Microwave-assisted synthesis (MAS) is widely adopted and regarded as an efficient and promising method for producing MOF materials because it allows for rapid and uniform heating of the entire reactant mixture in a short duration. Two programmable microfluidic syringe pumps are utilized to introduce metal salt and ligand precursor solutions into a PTFE tubular reactor in a microwave oven at the desirable reaction temperature. This setup enables the precursor solutions to traverse within a constrained space, promoting nucleation and crystal growth reactions. Vo *et al.* synthesized UiO-66 following this process.[36] Carrasco *et al.* synthesized PCN-222 *via* one-pot microwave-assisted synthesis.[37] MOF-808 with high porosity and a controlled crystal size can be easily prepared *via* a water-based microwave-assisted route.[38]

2.3 Sonochemical method

The ultrasonication or sonochemical technique has been employed for the synthesis of nanomaterials and the creation of mesoporous materials. Ultrasonication irradiation, in particular, stands out as an environmentally friendly alternative to traditional methods, offering a more rapid reaction process. The formation of cavities induced by waves generates localized hotspots within bubbles, thereby facilitating MOF synthesis. Zirconium tetrachloride ($ZrCl_4$) and 1,4-benzenedicarboxylic acid (H_2BDC) are both dissolved in a solution of dimethylformamide

Table 1 Distinctive examples of different Zr-MOFs with their mode of application in biomedical research

MOF	Cargos	Spectrum of ailments	Mode of action	Ref.
UiO-66	Doxorubicin	Hepatocellular carcinoma	Photothermal therapy (PTT), transcatheter arterial chemoembolization (TACE)	15
UiO-66-H_4Pc	Linezolid and lysozyme	Bacterial cell wall	Photodynamic therapy (PDT) and chemotherapy (CT)	48
Polydopamine (PDA) coated UiO-66	Perfluorotributylamine (PFA) and bioreductive prodrug tirapazamine (TPZ)	Hypoxia-activated osteosarcoma	PTT producing potent cytotoxic radicals	49
UiO-66-COOH	L-Methioninase		Anticancer activity	50
UiO-67 and NU-1000	Acriflavine (ACF)	SARS-CoV-2	Drug delivery	57
UiO-67 and MIL-100 (Fe)	Brimonidine	Glaucoma treatment	Drug delivery	58
PCN-222	Ab-DNA@PCN-222	Detection of prostate-specific antigen (PSA)	Photoelectrochemical (PEC) immunoassay	55
PCN-222	Bi NPs	Bactericidal	Radical oxygen species (ROS)	56
PVP-coated lanthanide-doped UCNPs combined with PCN-224	Generation of cytotoxic singlet oxygen ($^1O_2$)	Tumor cells	Cytotoxicity *via* PDT	59
UCNP-PCN-224	Generation of cytotoxic singlet oxygen ($^1O_2$)	Tumor cells	PDT	60
PCN-224 modified with DNA aptamers (AS1411)		MDA-MB-231 cells	PDT	61
Folic acid (FA) incorporated PCN-224 NMOFs	Folic acid (FA)	HeLa cells	PDT	62
PCN-224-DNA aptamer	Doxorubicin (DOX)	A549 lung cancer cells	Drug delivery and PDT	63
Pt-decorated PCN-224	Cytotoxic singlet oxygen ($^1O_2$)	H22 tumors	PDT	64
L-arginine (L-Arg)-incorporated PCN-224	L-Arg, a natural source of NO	4T1 cells	Gas therapy, generation of reactive oxygen species (ROS), PDT	65

(DMF). Subsequently, the two solutions are combined and agitated within a laboratory bottle. Ultrasonication is carried out for two hours at 120 °C using a handheld portable ultrasonic homogenizer probe. The resulting precipitate is thoroughly washed with DMF and methanol solutions, followed by drying in an oven at 90 °C.[39] Yu *et al.* synthesized MOF-525 using this process.[40]

2.4 Electrochemical method

The electrochemical synthesis of MOFs has emerged as a noteworthy synthetic approach, garnering significant attention from researchers due to its rapid and efficient performance under mild reaction conditions. Zhang *et al.* synthesized UiO-67 by following this method.[41] The necessary quantities of TATB and H_2BPDC were dissolved in DMSO using ultrasonic agitation. Zirconium sheets were employed as both the cathode and anode for the electrochemical synthesis, with the reaction voltage carefully adjusted. The resulting white precipitate in the solution underwent multiple washing steps and subsequent drying. UiO-66 is also synthesized by this process where the zirconium wire, stained on the surface, was subjected to pre-treatment washing to transform it into an anode, while the aluminum sheet underwent a similar treatment to be prepared as a cathode.[42]

2.5 Mechanochemical method

The mechanochemical ball-milling method is an efficient approach for synthesizing various significant MOFs. For example, microporous UiO-67 MOFs with surface areas of up to 2250 $m^2\ g^{-1}$ were achieved through a solvent-free mechanochemical process, utilizing dodecanuclear zirconium acetate clusters and H_2BPA (biphenyl-4,40-dicarboxylic acid) as the source materials for clusters and ligands, respectively.[43] Mechanochemical techniques have been proven to be highly suitable for the environmentally friendly and swift synthesis of MOF-525.[44]

3. Some important Zr-MOFs and their biomedical applications

Zr-based metal–organic frameworks with cytotoxicity and antibacterial activity have found extensive use in biomedicine, for various applications such as targeted drug delivery, photothermal therapy (PTT), photodynamic therapy (PDT), and bioimaging. The diverse range of porous MOF materials, resulting from different metal ions and linkers, address issues like poor selectivity and unwanted drug side effects. Zr-based MOFs exhibit notable stability at biological pH levels, enhancing their suitability for bio-imaging and other applications. Specifically, Zr-based UiO MOF platforms demonstrate the capability to deliver multiple cargo materials simultaneously. Lin and coworkers reported siRNA/UiO-Cis composites designed to deliver cisplatin and small interfering RNAs to address cisplatin-resistant ovarian cancer. They incorporated cisplatin within the pores of the MOF carriers and attached RNAs on the

surface. This co-delivery strategy demonstrates the feasibility of utilizing Zr-based MOFs and expanding their applications in biomedical research.[45]

Selecting appropriate ligands is crucial for achieving specific applications. MOF systems like PCN-222 and PCN-224, incorporating tetrakis(4-carboxyphenyl)porphyrin (TCPP) linkers capable of absorbing visible light, exhibit potential for application in photodynamic therapy (PDT) and photoelectrochemical (PEC) immunoassays. Among the numerous Zr-based MOFs reported in the literature, we have focused our attention on some important classes of Zr-MOFs that have excellent application potential in the biomedical field (Table 1).

3.1 UiO-66

The UiO-66 MOF was initially synthesized and reported by Lillerud's research group at the University of Oslo; hence, the name was derived from the university.[11] This Zr-based MOF is constructed using 1,4-benzenedicarboxylic acid (BDC) linkers. This MOF is known for its remarkable characteristics, including an exceptionally high surface area and impressive thermal stability, which can be attributed to the unique cuboctahedral structure of the metal oxide node coupled with the elevated coordination number that exists between the zirconium nodes and the organic bridges forming this particular MOF structure.[29] UiO-66 displays exceptional resistance to diverse solvents, remarkable stability when exposed to water, air, and chloroform, and remarkable resilience against external pressures. UiO-66 has gained significant recognition from the scientific community because of its exceptional tunability and functionality, which involve managing both missing-cluster and missing-linker defects. UiO-66 has gained extensive attention due to its potential as an adaptive carrier of pharmaceuticals within intelligent drug delivery systems, offering promising prospects for treating a spectrum of ailments. Notable examples encompass breast cancer, lung cancer, and colorectal cancer, as well as hypoxia-activated osteosarcoma. The modified UiO-MOFs not only show great promise in treating atherosclerotic cardiovascular disease, but also they serve as carriers for loading H_2S donors like GYY4137, enhancing therapeutic effects.[46,47]

Liu *et al.* utilized a solvothermal technique to create a carrier derived from UiO-66, which was loaded with doxorubicin.[15] This carrier was subsequently enhanced with Bi_2S_3 modification. The drug's release followed a pH-triggered model and exhibited photothermal characteristics in both *in vitro* and *in vivo* investigations. To assess its biocompatibility, cytotoxicity and hemocompatibility evaluations were conducted, yielding favourable results in terms of biocompatibility. In the context of transcatheter arterial chemoembolization (TACE), the primary treatment for hepatocellular carcinoma (HCC), researchers employed a rat N1S1 liver tumor model. Their findings indicated that a combination of PTT and TACE could effectively hinder tumor growth. This combination also demonstrated the ability to suppress angiogenesis, enhance apoptosis, and influence proliferation as part of the tumor response. Lv *et al.* devised an innovative and remarkably effective nanoplatform with multiple antibacterial properties.[48] This was accomplished through an amidation reaction that involved the utilization of tetra-(4-carboxyphenoxy)phthalocyanine zinc, an exceptionally active photosensitizer (PS), and UiO-66-NH_2 to construct a highly efficient carrier system for drugs. In a subsequent step, chemical antibacterial agents such as linezolid and lysozyme, a stable and biocompatible protein known for its robust resistance to high temperatures and acidic conditions, were loaded sequentially into the pores and onto the external surface of the MOF. This loading was achieved through electrostatic adsorption and molecular interactions creating a composite denoted as (Li@UiO-66-H_4Pc)@lysozyme. The immobilized lysozyme displayed a targeted interaction with the bacterial cell wall, leading to its disintegration. This interaction facilitated the entry of the nanomaterials into the bacterial cells, consequently enhancing the combined effectiveness of PDT and chemotherapy (CT) in a synergistic manner. Moreover, this approach mitigated the likelihood of bacterial resistance to the therapeutic agents. Chen and co-researchers innovated a microporous nanocarrier based on the MOF, which was enveloped in a polydopamine (PDA) coating, and within this structure, they encapsulated both perfluorotributylamine (PFA) and bioreductive prodrug tirapazamine (TPZ) for a specialized therapeutic approach targeted at hypoxia-activated osteosarcoma treatment.[49] The outlined scheme in Fig. 1 highlights the selection of UiO-66 as the optimal nanocarrier, chosen for its substantial surface area and exceptional porosity. This framework was employed to encapsulate both PFA and the prodrug TPZ. Following this, the engineered MOF nanoparticles underwent an additional step involving PDA coating, resulting in the final product, TPZ/PFA@UiO-66@PDA. Upon intravenous administration, TPZ/PFA@UiO-66@PDA efficiently accumulated within tumor tissue owing to the well-established enhanced permeability and retention (EPR) effect. Within this context, the PFA component present in TPZ/PFA@UiO-66@PDA effectively absorbs oxygen, thereby intensifying the hypoxic condition of the tumor microenvironment. The augmented tumor hypoxia consequently triggered the activation and conversion of the prodrug TPZ into potent cytotoxic radicals, prompting programmed cell death in the tumor cells. Additionally, the accumulation and internalization of the PDA coating further heightened tumor permeability, especially when subjected to 808 nm laser irradiation. This was instrumental in effectively targeting and eliminating drug-resistant tumor cells. The combined approach of TPZ/PFA@UiO-66@PDA nanoparticles achieved a synergistic effect by integrating hypoxia-activated bioreductive prodrug therapy with photothermal therapy (PTT), resulting in a potent strategy for effectively suppressing tumor growth.

Hassabo *et al.* have drawn a noteworthy conclusion regarding the unexpected role of L-methioninase@UiO-66-COOH in developing potential anticancer drugs.[50] They have uncovered an intriguing and unanticipated connection between L-methioninase and UiO-66-COOH, which holds promise for creating therapies to restrain tumor growth. The L-methioninase@UiO-66-COOH composite has demonstrated significant advancements in stability compared to the free enzyme. Notably, this composite displayed remarkable stability, maintaining its integrity at temperatures as high as 80 °C for approximately 40 min

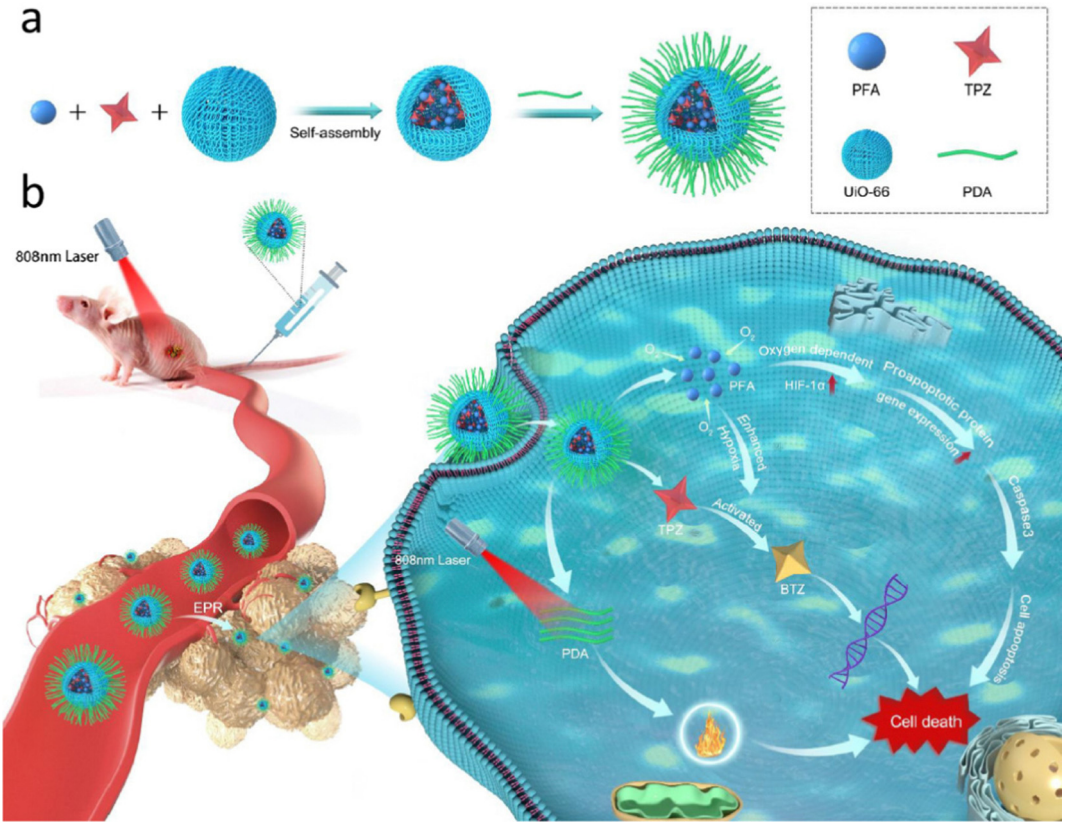

Fig. 1 (a) Diagram depicting the synthesis process of TPZ/PFA@UiO-66@PDA nanoparticles. (b) Administration of TPZ/PFA@UiO-66@PDA nanoparticles *via* tail vein injection followed by laser irradiation for targeted treatment of hypoxic osteosarcoma. Reproduced with permission from ref. 49 Copyright 2021 Springer.

and remaining stable within a pH range of 5 to 7. Moreover, L-methioninase@UiO-66-COOH exhibited substantial improvements in storage stability, retaining its functionality for more than twelve days. These findings highlight the potential of this composite in developing stable and effective anticancer treatments.

3.2 UiO-67

Besides UiO-66 and derived compounds another member of this MOF family is UiO-67 which has received immense attention from the scientific community. UiO-67 is also a Zr-based MOF supported by 4,4′-biphenyl dicarboxylic acid linkers.

Chen *et al.* have published findings on the utilization of UiO-67-NH_2 nanoparticles (using 2-amino-4,4′-biphenyl dicarboxylic acid linkers) with a size of 150 nm as a carrier material for the anticancer drug camptothecin (CPT).[51] The Nano-UiO-67-NH_2 particles demonstrated remarkable drug loading capacity (36.53 wt%) and efficient drug encapsulation (19.21%) when impregnated with CPT in the methanol solvent. Notably, the release study of CPT in PBS revealed a gradual drug release pattern, with a 74% release over five days, effectively avoiding any abrupt "burst" release. These results from the study of the adsorption and controlled release of the anticancer drug strongly suggest that nano-UiO-67-NH_2 holds promise for developing controlled drug delivery systems. Liu and colleagues have developed a novel multifunctional drug carrier, termed FUFP (5-FU@UiO67-$(NH)_2$-FAM/PMT) [where, 5-FU = 5-fluorouracil, 5-FAM = 5-carboxyfluorescein (fluorescence imaging agent), and PMT = pemetrexed (anti-tumor drug)] which is designed to enhance the cytotoxicity for cancer therapy through targeted delivery of bimodal drugs.[52] *In vitro* drug release studies revealed that FUFP displayed excellent structural stability and exhibited a slow drug release profile in deionized water, demonstrating biodegradability and efficient drug release in PBS media. Furthermore, cytotoxicity experiments demonstrated the potent antitumor activity of FUFP, highlighting its ability to produce synergistic antitumor effects through the combined action of 5-FU and PMT within the carrier. Utilizing fluorescence imaging and flow cytometry analysis, FUFP exhibited a strong folate-targeting capability. *In vivo* studies in nude mice with cervical cancer confirmed the significant tumor suppression achieved by FUFP, underscoring its impressive antitumor efficacy. Deng *et al.* synthesized Zr-Fc (ferrocene) MOF nanosheets with a lateral size of approximately 500 nm and a thickness of 16.4 nm, aiming to harness their potential for synergistic cancer therapy through photothermal therapy (PTT) and Fenton reaction-based chemodynamic therapy (CDT) (Fig. 2).[53] These Zr-Fc MOF nanosheets exhibit a consistent absorption spectrum spanning from 350 to 1350 nm and possess an exceptional photothermal conversion efficiency of 53% at 808 nm. Both *in vitro* and *in vivo* experiments confirm the remarkable photothermal properties of the Zr-Fc MOF

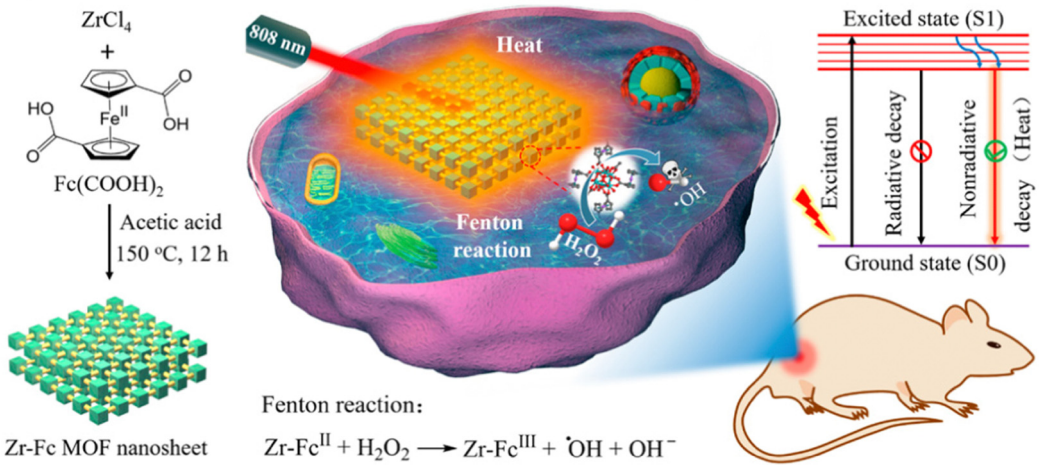

Fig. 2 Production of Zr-Fc MOF nanosheets and visual representation of combined photothermal therapy (PTT) and Fenton reaction-driven chemodynamic therapy (CDT) synergy. Reproduced with permission from ref. 53. Copyright 2020 American Chemical Society.

nanosheets, rendering them highly effective photothermal agents for PTT. Simultaneously, these Zr-Fc MOF nanosheets demonstrate efficient catalytic activity as Fenton catalysts, facilitating the generation of •OH radicals for CDT. Consequently, *in vitro* investigations substantiate the synergetic interplay between PTT and CDT, resulting in outstanding therapeutic outcomes. This synergistic effect of PTT and CDT has been successfully translated into promising therapeutic effects in cell culture studies and animal models. In summary, the authors have successfully established an "all-in-one" MOF-based platform for synergistic PTT and CDT in cancer treatment, capitalizing on the photothermal and catalytic attributes of the Zr-Fc MOF nanosheets. Notably, this platform eliminates the need for additional photothermal or chemotherapy agents, serving as an inspiring model for the development of other MOF-based synergistic cancer therapy platforms.

3.3 PCN-222

Immunoassays hold significant promise for the initial clinical detection of different tumors, including the utilization of prostate-specific antigen (PSA) analysis to diagnose prostate cancer. Photoelectrochemical (PEC) immunoassay stands as a prospective bio-analysis technique, relying on photoinduced electron transfer (PET) interactions between an analyte, photoactive components, and an electrode during photoirradiation. This method has found extensive application in identifying diverse biological molecules. MOFs with electrochemically active linkers are excellent candidates for potential therapeutic application in this field. PCN-222 belonging to the Zr-based MOF family is designed from highly stable Zr_6 clusters as nodes and tetrakis(4-carboxyphenyl)porphyrin (TCPP) linkers capable of absorbing visible light.[54] Moreover, the significant porosity and adjustable structures of PCN-222 offer the advantage of concentrating oxygen and dopamine (DA) molecules around the photoelectrochemically active TCPP ligands. This arrangement contributes to an augmentation of the efficiency of converting light into electricity. Additionally, as depicted in Fig. 3(A), the coordination of phosphate groups and inorganic Zr–O clusters within PCN-222 introduces steric hindrance effects. This characteristic enables the utilization of a PCN-222-modified electrode to detect phosphoproteins without requiring labels. Thus, PCN-222 and its derivatives have potential applications in photoelectrochemical (PEC) immunoassay.

Recently, Zhang *et al.* presented a novel non-enzyme photoelectrochemical (PEC) immunoassay utilizing DNA-mediated nanoscale PCN-222 for the purpose of detecting prostate-specific antigen (PSA).[55] The antibody tagged with single-stranded DNA (Ab-DNA) was linked to PCN-222, resulting in the formation of Ab-DNA-functionalized complexes known as NMOFs (nanoscale metal–organic frameworks). These Ab-DNA-NMOFs acted as active photocathode substrates in a PEC setup, exhibiting a significantly enhanced photocurrent response when exposed to dopamine (DA) in aqueous media containing oxygen. The cathodic photocurrent appeared in the presence of oxygen (Fig. 3(B), curve b), indicating its role as an electron acceptor in the PEC system. Dopamine further boosted the photocurrent response (Fig. 3(B), curve c), acting as an efficient electron donor. In the PCN-222 working mechanism (Fig. 3(C)), TCPP ligands on NMOFs are excited, leading to electron transfer and the generation of electron–hole pairs. Introduction of dopamine oxidizes them, scavenging holes and facilitating more electrons in the conduction band of NMOFs. This enhances electron transfer to oxygen, resulting in a stronger photocurrent signal. Essentially, dopamine inhibits electron–hole pair recombination, promoting electron transfer and enhancing cathodic photocurrent. Through additional modification with polyamidoamine dendrimers, the Ab-DNA-NMOFs demonstrated efficient signal transduction capabilities for PEC applications, enabling non-enzyme PSA immunoassays with impressive photoinduced thermal imaging (PTI) ability in living organisms.

Wu *et al.* reported the incorporation of bismuth NPs into PCN-222, resulting in the creation of Bi-PCN-222.[56] This novel biomimetic nanozyme catalyst features an interfacial Schottky

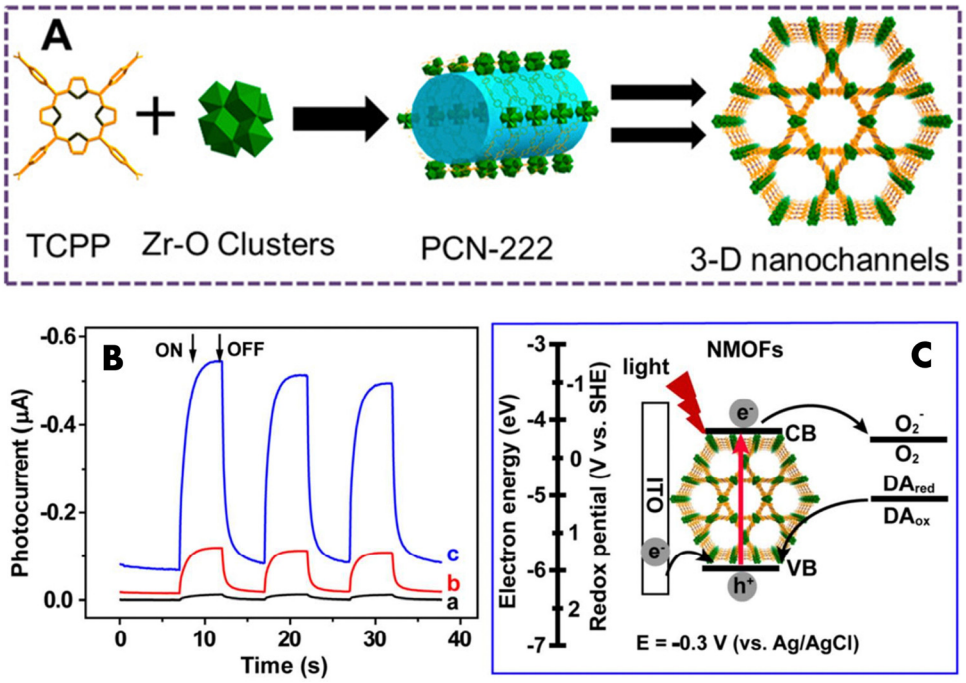

Fig. 3 (A) Diagrammatic representation of PCN-222 fabrication. Reproduced with permission from ref. 54. Copyright 2016 American Chemical Society. (B) Cathodic photocurrent after deoxygenation with N_2 for 20 min (carve a), 0 min (carve b), and 0 min + 1 mM dopamine (carve c) in 0.1 M HEPES buffer solution (pH 7.4) at $E = -0.3$ V (*vs.* Ag/AgCl). (C) The cathodic photocurrent generation mechanism, based on ITO/NMOFs. Reproduced with permission from ref. 55. Copyright 2016 American Chemical Society.

heterojunction structure. Remarkably, Bi-PCN-222 exhibited exceptional bactericidal efficacy, successfully eradicating 99.9% of *Staphylococcus aureus* (*S. aureus*). The mechanism behind this effect is the incorporation of Bi NPs, which endows the Bi-PCN-222 MOF with two crucial attributes: autonomous charge transfer facilitated by the Schottky interface, and the ability to mimic the activities of oxidase and peroxidase enzymes. In this context, the abundant free electrons interact with surrounding oxygen species to generate radical oxygen species (ROS) (Fig. 4). Moreover, when exposed to Bi-PCN-222 in a physiological setting, bacteria experience a disruption in their respiratory process and subsequent metabolism. This is due to Bi-PCN-222's optimal redox potential, which triggers electron transfer along bacterial membranes and into their interior through an electron transport pathway. The inability to pump protons from protein complex III to IV, where they would normally react with oxygen, leads to a reduced formation of ATP. As a result, bacterial function is compromised upon contact. Additionally, Bi-PCN-222 can enhance tissue regeneration by upregulating genes associated with fibroblast proliferation and angiogenesis (bFGF, VEGF, and HIF-1α), thereby fostering wound healing.

3.4 PCN-224

Another family of Zr(IV)-based MOF nanoparticles with exceptionally stable frameworks featuring three-dimensional intricate nanochannels, referred to as PCN-224, Zr(IV)-based porphyrinic MOF nanoparticles, has been constructed through a linker-elimination approach.[66] This synthesis involves the assembly of six-connected Zr_6 clusters and metalloporphyrins. Near-infrared (NIR) light offers distinct benefits compared to visible light, such as enhanced tissue penetration, heightened sensitivity, and improved resolution. These attributes make the utilization of porphyrin-based MOFs to harness NIR light or near-infrared-triggered PDT an appealing prospect. Researchers demonstrated the improved therapeutic efficacy of NIR-triggered PDT through the synergistic application of porphyrin-based MOFs and upconversion nanoparticles (UCNPs). Li *et al.* presented a novel approach in tumor therapy by introducing heterodimers named UCMOFs, which consisted of PVP-coated lanthanide-doped UCNPs combined with PCN-224.[59] These UCMOFs were designed to respond to NIR light, enabling tumor treatment. The UCNPs absorbed NIR light and emitted visible light, which was then utilized for transferring energy to the TCPP molecule within PCN-224, leading to the generation of singlet oxygen ($^1O_2$). Intriguingly, the research findings demonstrated that upon exposure to 980 nm laser irradiation, UCMOFs generated cytotoxic $^1O_2$ instead of relying solely on PCN-224. Furthermore, the efficacy of this approach was corroborated through *in vivo* tests assessing antitumor activity. These experiments solidly confirmed the substantial ability of UCMOFs to apply them in NIR-triggered PDT. This innovative strategy presents a viable route for leveraging porphyrin-based MOFs capable of harvesting NIR light, thereby enabling effective NIR-triggered PDT for treating large or deeply situated tumors. He *et al.* achieved a significant advancement by creating core–shell nanoparticles combining the MOF (PCN-224) and UCNPs through DNA-mediated assembly.[60] Under NIR laser exposure, these MOF-UCNP nanoparticles exhibited the capability to generate $^1O_2$, and this production increased proportionally with

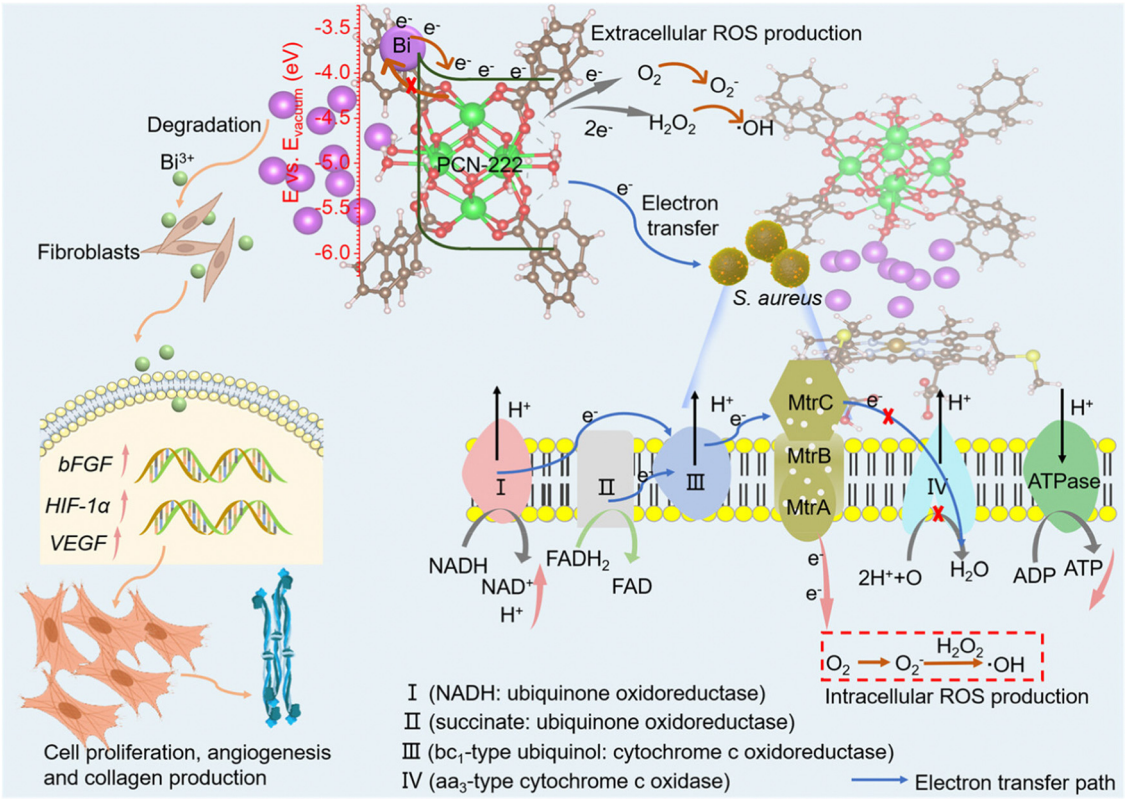

Fig. 4 Diagram illustrating the antibacterial mechanism and enhancement of cell proliferation and differentiation for accelerated wound healing. Reproduced with permission from ref. 56. Copyright 2023 American Chemical Society.

the UCNPs' loading (Fig. 5(a)). The experimental outcomes unveiled that when subjected to 980 nm laser irradiation, PCN-224 alone (without UCNPs) resulted in comparatively lower cell death. In contrast, the application of NIR irradiation to MOF-UCNPs led to a remarkable reduction of 63.7% in cell viability. This stark difference underscores the immense potential of MOF-UCNP nanoparticles as a formidable candidate for near-infrared-triggered PDT. Furthermore, the incorporation of distinct biomolecules like cell membranes, DNA, and antibodies into porphyrinic MOFs also yields the capability of active targeting. Ning *et al.* devised a universal approach for DNA functionalization of MOFs using surface coordination chemistry. They then extended this technique to modify PCN-224 NMOFs with DNA aptamers (AS1411). This modification endowed PCN-224 NMOFs with the ability to specifically recognize molecules, enabling targeted interaction with human breast cancer cells MDA-MB-231.[61]

The size of NMOFs is highly significant in relation to cellular uptake as the efficacy of PDT increases based on how much photosensitizers are absorbed by tumor cells, which is also influenced by their accumulation within tumor tissues. To study this effect, Park and colleagues synthesized PCN-224 particles spanning sizes between 30 and 190 nm (Fig. 5(b)), aiming to explore the impact of particle dimensions on both cellular intake and the effectiveness of PDT.[62] The PCN-224 nanoparticles demonstrated varying degrees of uptake within HeLa cells. Notably, the 90 nm version of PCN-224 exhibited the highest cellular uptake, as ascertained through inductively coupled plasma mass spectrometry (ICP-MS) (Fig. 5(c) and (d)). Moreover, in PDT for HeLa cells, the 90 nm PCN-224 variant notably prompted a significant 81% increase in cell apoptosis post-PDT treatment. This percentage was considerably more significant than the apoptosis induced by PCN-224 nanoparticles of other sizes. This outcome suggests that the effectiveness of PDT is influenced by the size-dependent cellular uptake of these nanostructured metal–organic frameworks (NMOFs). Moreover, the PCN-224 NMOFs were customized by incorporating folic acid (FA), a ligand that binds to the overexpressed folate receptor (FAR) on tumor cells. This binding is facilitated by the interaction between the carboxylate groups of FA and the Zr_6 clusters within the NMOFs. The findings revealed that the FA-modified PCN-224 NMOFs exhibited enhanced cellular uptake by FAR-positive HeLa cells compared to unmodified PCN-224 NMOFs. This improved uptake was attributed to the FA receptor-mediated endocytosis. Furthermore, this modification led to a heightened PDT effectiveness against HeLa cells.

Zhang *et al.* have illustrated using DNA-functionalized NMOFs to track tumor cells, targeting explicitly through drug delivery and PDT.[63] It is widely recognized that the structure and dimensions of NMOFs substantially impact their drug-loading capabilities and potential for cellular uptake. Therefore, the controlled synthesis of NMOFs with precise sizes is of paramount importance. In Fig. 5(e), a schematic representation illustrates the creation of nanoscale PCN-224 using 5,10,15,20-tetrakis(4-carboxyphenyl)porphyrin (TCPP), benzoic acid, *N*,*N*-

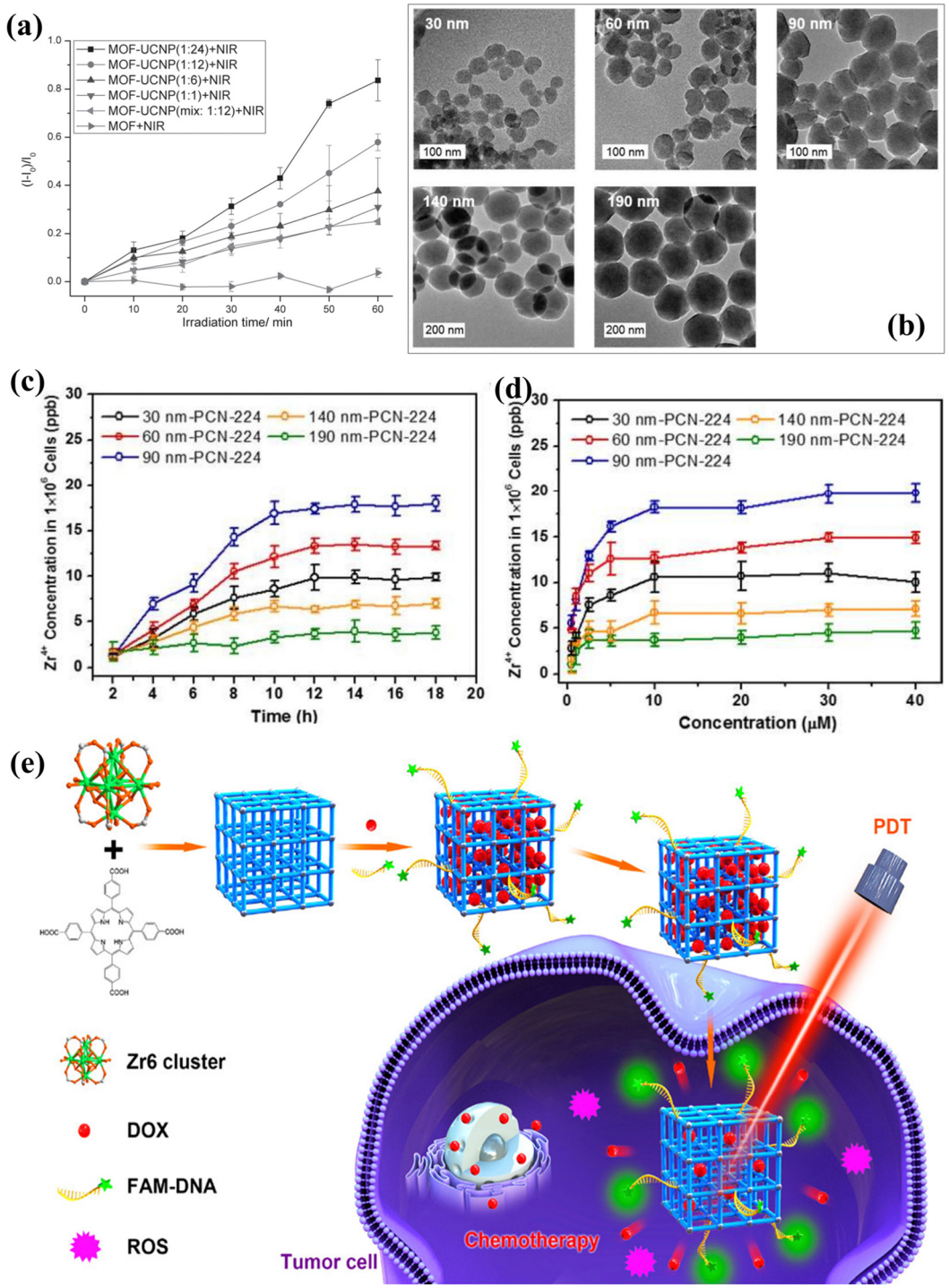

Fig. 5 (a) Singlet oxygen production was examined under 980 nm laser irradiation for MOF NPs, MOF-UCNP mixtures, and DNA-assembled MOF-UCNP core–satellite superstructures at varying MOF:UCNP molar ratios. Reproduced with permission from ref. 60. Copyright 2017 Wiley. (b) TEM images of PCN-224 nanoparticles ranging from 30 to 190 nm. Cellular uptake of varied-sized PCN-224 samples assessed over different (c) incubation times and (d) concentrations (incubation time 24 h), measured *via* ICP analysis of Zr concentration in HeLa cells. Reproduced with permission from ref. 62. Copyright 2016 American Chemical Society. (e) Diagram depicting DNA-modified PCN-224 for tumor cell imaging, targeting drug delivery, and PDT. Reproduced with permission from ref. 63. Copyright 2019 American Chemical Society.

dimethylformamide, and biocompatible Zr^{4+} ions *via* a stirring method. This nanomaterial served as a carrier for doxorubicin (DOX), which is frequently used as a model antitumor drug to assess loading capacity and pH-responsive release characteristics. Following the loading of DOX, the system underwent functionalization with an aptamer (DNA) specifically designed for A549 lung cancer cells. The A549 cell aptamer exhibits a robust affinity and high specificity for A549 cells.

Furthermore, carboxyl and fluorescein modifications were introduced at the aptamer's two terminals. The carboxyl group formed a coordination bond with Zr^{6+} ions, resulting in the creation of DNA-functionalized PCN-224. The fluorescein component facilitated the tracking of A549 cells by binding to PCN-224-DNA. Upon contact with A549 cells, DOX@PCN-224-DNA proved effective in tracking tumor cells and demonstrated targeted therapy capabilities, combining chemotherapy and photodynamic therapy. This straightforward approach to aptamer functionalization of PCN-224 holds promise for the development of metal–organic framework-based targeted therapies and biosensors.

Porphyrins exhibit significant promise in the context of PDT; however, the reliance on oxygen restricts the effectiveness of PDT due to the prevalence of hypoxic conditions within the majority of tumor cells and tissues. To enhance the effectiveness of PDT by improving intra-tumoral oxygen levels and addressing hypoxia in a tumor microenvironment, a promising approach involves the integration of MOFs with supplementary agents like oxygen carriers, peroxidase, and oxygen consuming interference agents. Alternatively, the intrinsic components of MOFs, such as Cu, Fe, and Mn metal ions within their skeletons, can be utilized for Fenton-like reactions. This integrated strategy offers an efficient means of surmounting hypoxia, elevating intratumoral oxygen concentrations, and consequently achieving heightened therapeutic efficacy in PDT. Zhang *et al.* introduced a novel approach involving Pt-decorated PCN-224 (PCN-224-Pt) nanostructures to enhance PDT.[64] By capitalizing on the elevated levels of H_2O_2 within the tumor microenvironment, platinum nanoparticles endowed with catalase-like properties exhibited the ability to catalyze the breakdown of intratumoral H_2O_2, leading to the generation of oxygen (O_2). This, in turn, facilitated the subsequent production of cytotoxic singlet oxygen ($^1O_2$), which played a crucial role in eradicating tumor cells. In laboratory settings, *in vitro* outcomes highlighted that PCN-224-Pt induced notably greater cell lethality under hypoxic conditions when subjected to 638 nm laser irradiation compared to PCN-224 alone. Furthermore, the *in vivo* efficacy of PCN-224-Pt was assessed using a mice model with H22 tumors. The results unequivocally demonstrated that the injection of PCN-224-Pt followed by irradiation inhibited tumor growth. In contrast, when PDT was applied using PCN-224 alone, only partial suppression of tumor growth was observed.

Gas therapy has emerged as a promising avenue for tumor treatment, owing to its minimal adverse effects and amplified therapeutic effectiveness. Diverse gaseous transmitters like hydrogen sulfide (H_2S), nitric oxide (NO), and carbon monoxide (CO) have found applications in gas therapy. These transmitters hold the potential to expedite the apoptosis of tumor cells, impede the proliferation of these cells, and carefully preserve the activity and physiological functioning of normal cells selectively. Wan *et al.* introduced an innovative approach involving the combined utilization of nitric oxide (NO) gas therapy and PDT for tumor treatment.[65] This strategy hinged on L-arginine (L-Arg)-incorporated PCN-224 NMOFs. The presence of L-Arg, a natural source of NO, enabled the release of NO for gas therapy, a process facilitated by the oxidative action of reactive oxygen species (ROS) generated through PDT using PCN-224 upon exposure to 660 nm light. *In vitro*, experimentation through an MTT assay underscored that the viability of 4T1 cells treated with L-Arg-incorporated PCN-224 was notably lower than that of cells treated solely with PCN-224 when subjected to 660 nm light irradiation. Importantly, a flow cytometry-based cell apoptosis assay demonstrated that L-Arg-incorporated PCN-224 exhibited enhanced efficacy in PDT under hypoxic conditions compared to pure PCN-224. This observation substantiated the notion that NO sensitizes PDT within hypoxic tumor environments. Furthermore, an *in vivo* study evaluating antitumor effects indicated that the therapeutic potency of PCN-224 was surpassed by that of L-Arg-incorporated PCN-224 when both were exposed to 660 nm light. This outcome highlighted that the combined action of PDT and gas therapy yielded superior antitumor effects to a certain degree. This unique nanoplatform strategy, coupling gas therapy and PDT, introduces a novel therapeutic paradigm capable of surmounting the challenge of hypoxia in order to achieve more effective tumor treatment.

3.5 MOF-525

MOF-525 is a compelling Zr-based porous metal–organic framework (Zr-PMOF) initially synthesized by Morris and colleagues.[18] This material is formed from a 12-connected Zr secondary building unit (SBU) denoted as $[Zr_6O_4(OH)_4]$ and a TCPP linker. Notably, MOF-525 has an impressive BET surface area of 2620 $m^2\ g^{-1}$ and a pore size measuring 2.0 nm, the highest reported among Zr-MOFs at that time. Much like its Zr-MOF counterparts, MOF-525 exhibits remarkable chemical stability in acidic and aqueous environments. Furthermore, the TCPP linker within MOF-525 can host isolated single catalytic sites. Consequently, MOF-525 has attracted attention for a range of applications, including its use as a catalyst for CO_2 fixation and alkene epoxidation, as well as its application as a supercapacitor and cathode material in solar cells. The remarkable adsorption capabilities of MOF-525 are attributed to its high specific surface area and the presence of porphine, phenyl, and carboxyl groups. Notably, MOF-525 demonstrates the ability to adsorb single-stranded nucleic acids. Furthermore, it maintains consistent red fluorescence emission when excited. This characteristic presents an exciting opportunity to develop a ratiometric fluorescent biosensor using MOF-525. This biosensor could offer sensitive detection of miRNAs due to these unique attributes. A logically designed fluorescent biosensor was reported to detect the levels of exosomal miR-92a-3p.[67] This biosensor utilized MOF-525 with inherent fluorescence, which played a dual role as a fluorescence reference material and a quencher for the fluorescence emitted by a single-stranded reporter through adsorption. The presence of miR-92a-3p initiated a process where the 5P-template strand formed loops, followed by periodic rolling circle amplification (Fig. 6(a)). This amplification resulted in longer periodic strands that combined with the reporters, preventing their adsorption by MOF-525. The non-denaturing polyacrylamide gel electrophoresis analysis confirmed the formation of closed-loop structures and the periodic long strands as

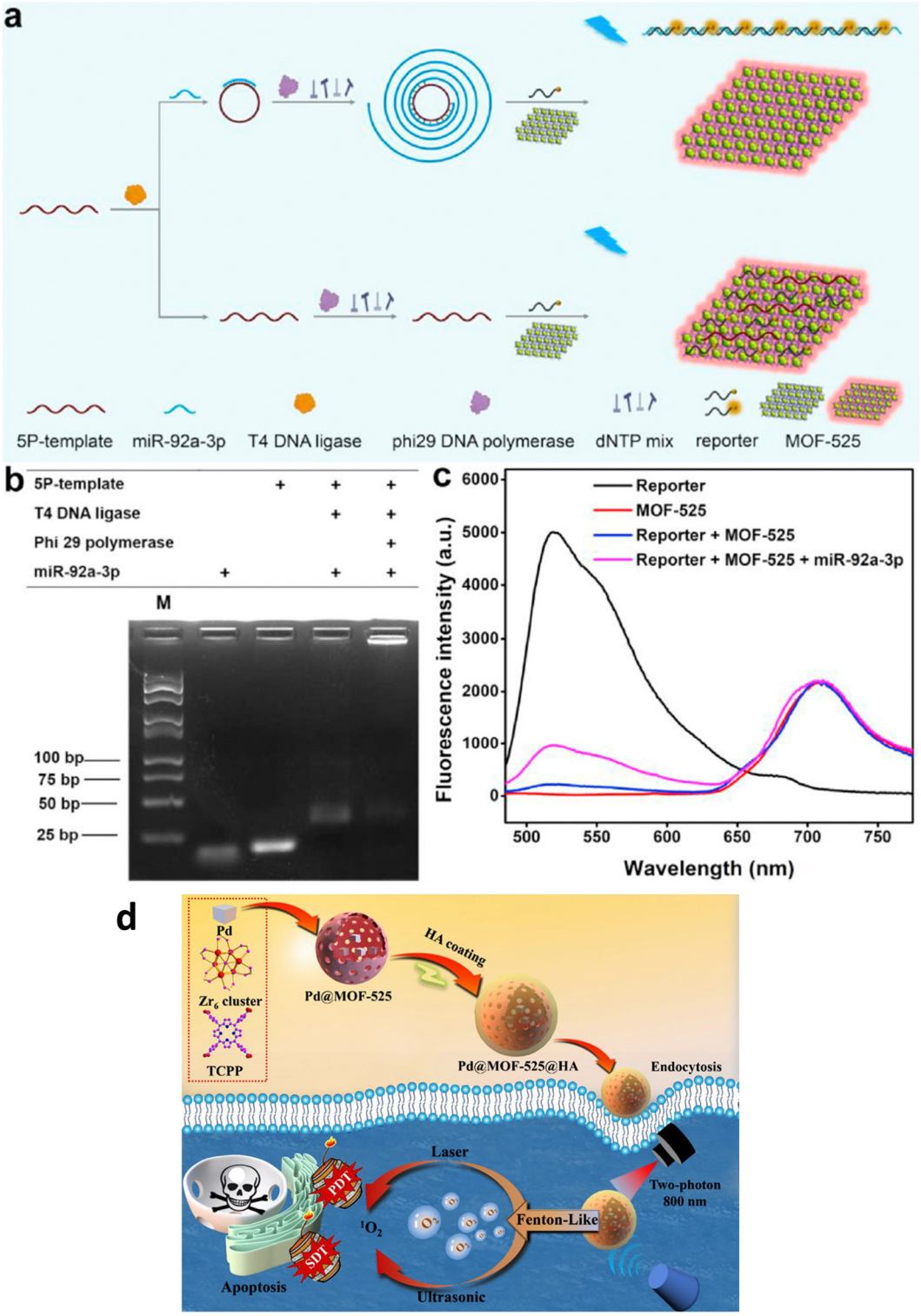

Fig. 6 (a) Detection process of miR-92a-3p. (b) Non-denaturing polyacrylamide gel electrophoresis image. (c) Fluorescence spectra of the reporter and MOF-525, and their combinations with miR-92a-3p. Reproduced with permission from ref. 67. Copyright 2022 Elsevier. (d) Illustration depicting the creation of Pd@MOF-525@HA, emphasizing the enhanced photodynamic and sonodynamic therapy. Reproduced with permission from ref. 69. Copyright 2022 Springer.

well (Fig. 6(b)). The concentration of miR-92a-3p was directly related to the fluorescence intensity ratio between the reporters and MOF-525 (Δreporter/MOF-525) (Fig. 6(c)). The biosensor had a detection range spanning from 0.1 to 10 pM and could distinguish miR-92a-3p from RNA sequences that do not match. To assess its effectiveness and feasibility in detecting exosomal

miRNA, the biosensor's results were compared with those obtained through traditional RT-qPCR (reverse transcription quantitative polymerase chain reaction), revealing close agreement between the two methods.

To monitor the release of dopamine (DA) from viable cells, Wu and coworkers developed an electrochemical biosensor employing a combination of porphyrinic MOFs (MOF-525) and poly(3,4-ethylenedioxythiophene) nanotubes (PEDOT NTs).[68] The cooperative enhancement of conductivity and catalytic efficiency of MOF-525-PEDOT NTs significantly strengthened the sensor's ability to detect dopamine. The biosensor exhibited a linear measurement range spanning from 2–270 μM, achieving a remarkable detection limit of 0.04 μM, for the dopamine concentration.

In addressing the challenge of hypoxia-associated anti-tumor therapy, Duan and coworkers developed a nanoplatform, Pd@MOF-525@HA, utilizing a Fenton-like reaction for oxygen generation (Fig. 6(d)).[69] This nanomaterial combines the oxygen-generating ability of Pd nanocubes within MOF-525 with the singlet oxygen production of porphyrinic MOF-525, enabling enhanced oxygen-dependent anti-tumor therapy through photodynamic and sonodynamic mechanisms. Surface modification involving hyaluronic acid (HA) wrapping significantly enhances biocompatibility and enables specific targeting of cancer cells. Additionally, Pd@MOF-525@HA exhibits two-photon activity, cancer cell-specific targeting, and near-infrared light-induced fluorescence imaging, facilitating precise guidance for cancer therapy with improved tissue penetration.

3.6 MOF-808

Furukawa *et al.* prepared MOF-808 for the first time to evaluate the water sorption properties of the MOF.[70] This MOF structure resulted from the assembly of Zr_6 metal nodes and 1,3,5-benzenetricarboxylic acid and has the molecular formula $Zr_6O_4(OH)_4(BTC)_2(HCOO)_6$. It exhibited the maximum BET surface area of 2060 $m^2\ g^{-1}$ with a pore volume of 0.84 cc g^{-1} and a pore diameter of 18.4 Å.

Nanoscale Zr-based MOFs like MOF-808 exhibit notable advantages in the realm of biomedical applications due to their exceptional characteristics, including high porosity, stability, and biocompatibility. Duman *et al.* investigated a highly efficient dual drug delivery system utilizing MOF-808 nanoparticles loaded with floxuridine (FUDR) and carboplatin (CARB) for cancer cell targeting (Fig. 7).[71] To further enhance selectivity and therapeutic efficacy, they coated these nanoparticles with a poly(acrylic acid-mannose acrylamide) (PAAMAM) glycopolymer. The findings reveal that MOF-808 not only amplifies the individual therapeutic effects of FUDR and CARB against cancer cells but also generates a synergistic effect when both drugs are combined, significantly boosting the cytotoxicity compared to free drug formulations. Moreover, the group demonstrated that modifying the activation protocol could increase CARB loading within the MOFs, thereby enhancing its cytotoxicity. The PAAMAM glycopolymer coating of MOF-808 substantially improved nanoparticle uptake by the cancer cells under investigation, particularly showcasing exceptional selective drug delivery with substantial cytotoxicity in HepG2 human hepatocellular carcinoma cells (half maximal inhibitory concentration, IC_{50} = (FUDR + CARB)@MOF-808 and PAAMAM@(FUDR + CARB)@MOF-808 reduces IC_{50} from 3.9 μg mL^{-1} to 2.4 μg mL^{-1}). These results underscore the potential for enhanced cytotoxicity through nanovector delivery and synergistic treatment, affirming MOF-808 as a promising candidate for future drug delivery research endeavours.

Parsaei and co-workers synthesized QU@MOF-808@CS-FA nanoparticles as targeted drug delivery vehicles for tumor therapy.[72] Encapsulation of quercetin (QU) within the MOF-

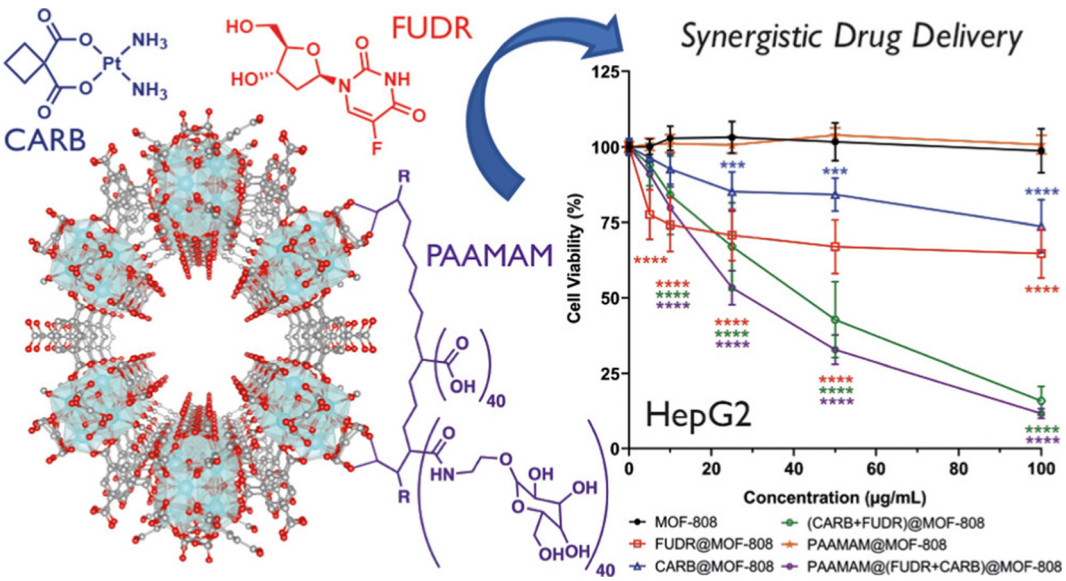

Fig. 7 Visualization of MOF-808's packing arrangement; chemical structures of chemotherapeutic compounds carboplatin (CARB) and floxuridine (FUDR), and glycopolymer poly(acrylic acid-mannose acrylamide) (PAAMAM); assessment of cell viability in HepG2 Cells following treatment with MOF-808, as well as its drug-loaded and PAAMAM-coated variants. Reproduced with permission from ref. 71. Copyright 2022 American Chemical Society.

808 shell was successfully achieved using the folic acid–chitosan (FA–CS) conjugate. Chitosan (CS) served as both a modifying and stabilizing agent, while folic acid (FA) was introduced as a potential targeting ligand for folate receptors (FRs). They also investigated its effectiveness as a smart carrier for QU. Additionally, they employed Monte Carlo simulations to gain insights into the drug–host interactions. According to the Monte Carlo simulation results, radial distribution function (RDF) analysis, and configuration snapshot analysis, hydrogen-bonding interactions emerged as the most influential factors governing QU loading onto MOF-808. To assess the *in vitro* cytotoxicity of QU, MOF-808, QU@MOF-808, and QU@MOF-808@CS-FA, they conducted MTT assays using both FR-negative HEK-293 (normal) cells and FR-positive MCF7 (cancer) cells. The outcomes not only confirmed the nanoparticles' internalization efficiency but also highlighted their cytotoxic and apoptosis-inducing properties. The designed modified nanocarrier offers several advantages, including a cost-effective and straightforward preparation process, short-term stability, long-term instability for extended drug release in acidic tumor environments, and active tumor targeting enabled by the high FA-binding affinity of FRs on tumor cell surfaces. These findings underscore the potential of MOF-808 functionalized with CS-FA as a superior platform for delivering QU and similar chemotherapeutics, holding promising prospects in targeted tumor therapies.

Biswas *et al.* successfully developed a label-free electrochemical immunosensor platform based on SA-functionalized MOF-808/CNT to detect the CA 125 ovarian cancer biomarker.[73] This platform was designed to enhance the electroconductivity and catalytic activity of MOF-808, achieved through compositing with carbon nanotubes (CNTs). The MOF-808/CNT-modified glassy carbon electrode (GCE) exhibited an exceptional electrochemical surface area (0.243 cm^2), outstanding charge transfer capabilities, and excellent electrocatalytic properties. Moreover, the synergistic combination of biocompatibility and remarkable electrochemical features in the MOF-808/CNT composite paved the way for an advanced label-free immunoassay platform for detecting CA 125. This immunoassay approach involved immobilizing captured antibodies onto MOF-808/CNT through a biotin-avidin system, simplifying the process and reducing the incubation time without compromising sensitivity. The developed immunosensor displayed a broad linear detection range (0.001–30 ng mL^{-1}) under optimized conditions, exhibiting the highest sensitivity at 43.88 μA ng^{-1} mL^{-1} and an astonishingly low detection limit of 0.5 pg mL^{-1}. Regarding sensor characteristics, the fabricated device exhibited reasonable reproducibility (RSD 99.3%), selectivity, and robustness. Analysis of patient serum samples yielded recoveries ranging from 105% to 110%, showcasing the significant potential of this immunosensor for clinical applications. Overall, the MOF-808/CNT composite opens up a versatile and promising avenue for developing immunoassay applications, particularly in the realm of CA 125 detection for ovarian cancer diagnosis and monitoring.

3.7 NU-1000

NU-1000 (NU = Northwestern University) is a renowned mesoporous MOF with pore sizes exceeding 2 nm. Zhao *et al.* prepared NU-1000 nanoparticles with varying sizes by using different solvents.[74] These NU-1000 nanoparticles exhibited a high BET surface area and a large pore volume, enabling a substantial drug loading capacity for doxorubicin hydrochloride (DOX), approximately 35 wt%. Furthermore, they exhibited a sustained release of the drug over an extended period, with over 60% release occurring over approximately two weeks. Due to NU-1000's excellent biocompatibility and the impressive anticancer efficacy of the drug-loading system, the resulting DOX@NU-1000@PEG formulation efficiently inhibited tumor growth. Both *in vitro* and *in vivo* tests demonstrated the substantial potential of NU-1000 as a drug carrier for chemotherapy, opening up new avenues for its applications in biomedicine.

Uremic toxins tend to accumulate more in individuals with impaired kidney function, such as those suffering from chronic kidney disease (CKD), leading to significant clinical complications that can result in severe illness or even death. Achieving effective removal of these toxins from the bloodstream is crucial for enhancing patients' hemodialysis success and ultimately improving CKD patients' survival rates. To achieve this, a comprehensive understanding of the interactions between an adsorbent material and uremic toxins is imperative for the development of efficient materials capable of eliminating these harmful compounds. Kato *et al.* investigated the adsorption behaviour of three uremic toxins: *p*-cresyl sulfate, indoxyl sulfate, and hippuric acid using a series of Zr-MOFs. Among the MOFs examined, NU-1000, a pyrene-based MOF, exhibits the highest efficiency in removing these toxins (Fig. 8).[75] In this MOF, two types of pores are available for adsorption of *p*-cresyl sulfate: the large mesopores (hexagonal; site 1) and small pores (triangular; site 2) both capable of providing π–π interactions for the effective inclusion of the adsorbate. Besides facilitating π–π interactions, the hydroxyl groups on the metal nodes establish hydrogen bonding interactions with the ionic functions of the adsorbate resulting in extremely high intake of *p*-cresyl sulfate by NU-1000. The appropriate positioning of the pyrene units of the linker is crucial in maximizing the extent of the interaction. This requires appropriate designing of the topology to arrest the adsorbate.

4. Conclusion and future perspectives

More than a decade has passed since the first report of UiO-66, and several other Zr-based MOFs have been developed. Due to their low toxicity and excellent biocompatibility, these MOFs are excellent candidates for application in biomedical research. The choice of an organic linker is very crucial in order to achieve a desirable working platform. Ligands like BDC, BTC and 4,4′-biphenyl dicarboxylic in UiO-66, MOF-808 and UiO-67, respectively, are proven to exhibit potential for effective drug delivery and photodynamic therapeutic application whereas the photoelectrochemically active TCPP ligands in porphyrinic MOFs such as PCN-222 and PCN-224 pave the path for their application in photoelectrochemical immunoassay. This class of porphyrinic MOFs also found potential applications in

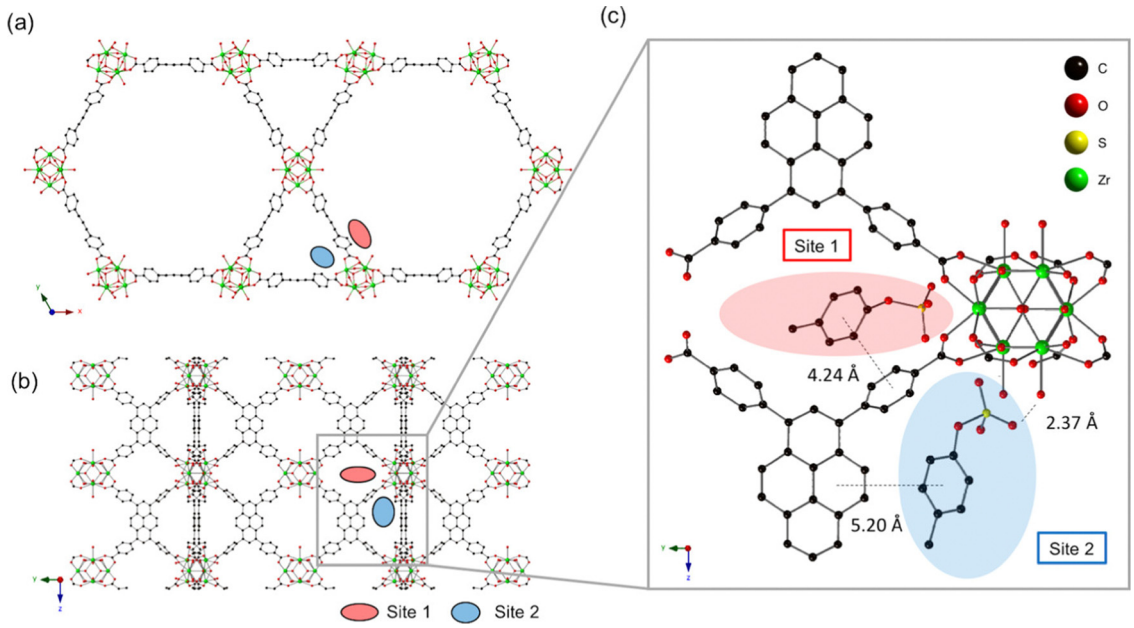

Fig. 8 (a) The crystal structure of NU-1000 viewed down the *c*-axis and (b) an orthogonal view prior to *p*-cresyl sulfate exposure (each adsorption site is depicted by a colored oval). (c) Optimized geometry of *p*-cresyl sulfate-pyrene and Zr_6 node domains after *p*-cresyl sulfate adsorption. Reproduced with permission from ref. 75. Copyright 2019 American Chemical Society.

photodynamic therapy and gas therapy. MOF-808 is a potential candidate for the construction of fluorescent biosensors. Thus, it is evident that the functionality of the linker backbone of a MOF is to be fine-tuned in order to achieve desirable applications. The linker dimension significantly controls the pore size of a MOF structure which in turn is of prime importance for its drug loading and releasing efficiency. In contrast, ligands with high electron densities and excellent luminescent properties are favoured for photochemical applications. This review compares the various types of linker-based MOFs and their effectiveness in bio-related applications in a single article in an ordered and compact manner.

In the future, the development of Zr-MOFs can progress in the following ways: (i) exploring the combination of Zr ions with different types of organic ligands to generate novel categories of Zr-MOFs; employing eco-friendly and a sustainable technique in the synthesis of MOFs is a crucial stride towards their commercial viability and broad application. Despite notable advancements in the synthetic methods, there remains ample opportunity for further enhancement. (ii) Integrating Zr-MOFs with emerging delivery vehicle systems to enhance material performance. Thorough exploration is imperative to achieve efficient drug delivery through various stimuli, encompassing glutathione (GSH)-responsive, glucose, H_2S, magnetic, pressure, and thermal triggers, among others. Additionally, a comprehensive examination of the *in vivo* degradation mechanisms and pathways of MOFs is essential; and (iii) currently, most research on Zr-MOFs is focused on applied research, with limited fundamental studies. Future basic investigations should explore the safety aspects and treatment mechanisms, expanding our understanding of Zr-MOFs.

Conflicts of interest

There are no conflicts to declare.

Acknowledgements

K. C. acknowledges Ishaan Mandal for allowing enough time for the literature survey and writing the draft. K. C. is also thankful to DST, India for financial support. M. M. thanks S. C. College, Habra, for permitting to carry out the research.

References

1 X. Ma, M. Lepoitevin and C. Serre, *Mater. Chem. Front.*, 2021, **5**, 5573–5594.
2 A. Ahmed, D. McHugh and C. Papatriantafyllopoulou, *Molecules*, 2022, **27**, 6585.
3 M. Moharramnejad, A. Ehsani, M. Shahi, S. Gharanli, H. Saremi, R. E. Malekshah, Z. S. Basmenj, S. Salmani and M. Mohammadi, *J. Drug Delivery Sci. Technol.*, 2023, 104285.
4 C. Jiang, X. Wang, Y. Ouyang, K. Lu, W. Jiang, H. Xu, X. Wei, Z. Wang, F. Dai and D. Sun, *Nanoscale Adv.*, 2022, **4**, 2077–2089.
5 C. Z. Dinu and H. Pham, *RSC Sustainability*, 2023, **1**, 1125–1149.
6 J. Munawar, M. S. Khan, S. E. Z. Syeda, S. Nawaz, F. A. Janjhi, H. U. Haq, E. U. Rashid, T. Jesionowski and M. Bilal, *Inorg. Chem. Commun.*, 2023, **147**, 110145.
7 X. Chen, M. Li, M. Lin, C. Lu, A. Kumar, Y. Pan, J. Liu and Y. Peng, *J. Mater. Chem. B*, 2023, **11**, 5693–5714.
8 M. Li, S. Yin, M. Lin, X. Chen, Y. Pan, Y. Peng, J. Sun, A. Kumar and J. Liu, *J. Mater. Chem. B*, 2022, **10**, 5105–5128.

9 I. A. Lazaro and R. S. Forgan, *Coord. Chem. Rev.*, 2019, **380**, 230–259.
10 D. B. Lee, M. Roberts, C. G. Bluchel and R. A. Odell, *ASAIO J.*, 2010, **56**, 550–556.
11 J. H. Cavka, S. Jakobsen, U. Olsbye, N. Guillou, C. Lamberti, S. Bordiga and K. P. Lillerud, *J. Am. Chem. Soc.*, 2008, **130**, 13850–13851.
12 J. Santos, M. T. Quimque, R. A. Liman, J. C. Agbay, A. P. G. Macabeo, M. J. A. Corpuz, Y. M. Wang, T. T. Lu, C. H. Lin and O. B. Villaflores, *ACS Omega*, 2021, **6**, 24382–24396.
13 H. Dong, G. X. Yang, X. Zhang, X. B. Meng, J. L. Sheng, X. J. Sun, Y. J. Feng and F. M. Zhang, *Chem. – Eur. J.*, 2018, **24**, 17148–17154.
14 D. Chen, D. Yang, C. A. Dougherty, W. Lu, H. Wu, X. He, T. Cai, M. E. Van Dort, B. D. Ross and H. Hong, *ACS Nano*, 2017, **11**, 4315–4327.
15 L. Liu, J. Zhuang, J. Tan, T. Liu, W. Fan, Y. Zhang and J. Li, *ACS Appl. Mater. Interfaces*, 2022, **14**, 7579–7591.
16 D. Fu, Y. Wang, J. Xu and H. Wu, *J. Solid State Chem.*, 2022, **310**, 123029.
17 D. Feng, Z. Y. Gu, J. R. Li, H. L. Jiang, Z. Wei and H. C. Zhou, *Angew. Chem.*, 2012, **124**, 10453–10456.
18 W. Morris, B. Volosskiy, S. Demir, F. Gándara, P. L. McGrier, H. Furukawa, D. Cascio, J. F. Stoddart and O. M. Yaghi, *Inorg. Chem.*, 2012, **51**, 6443–6445.
19 N. Rabiee, *Mater. Today Commun.*, 2023, **35**, 106244.
20 L. Wang, Z. Li, Y. Wang, M. Gao, T. He, Y. Zhan and Z. Li, *Nanoscale*, 2023, **15**, 10529–10557.
21 S. F. Fatima, R. Sabouni, R. Garg and H. Gomaa, *Colloids Surf., B*, 2023, **225**, 113266.
22 P. Wiśniewska, J. Haponiuk, M. R. Saeb, N. Rabiee and S. A. Bencherif, *Chem. Eng. J.*, 2023, **471**, 144400.
23 L. He, M. Shang, Z. Chen and Z. Yang, *Chem. Rec.*, 2023, **23**, e202300018.
24 M. Moharramnejad, R. E. Malekshah, A. Ehsani, S. Gharanli, M. Shahi, S. A. Alvan, Z. Salariyeh, M. N. Azadani, J. Haribabu, Z. S. Basmenj and A. Khaleghian, *Adv. Colloid Interface Sci.*, 2023, **316**, 102908.
25 H. Q. Zheng, Y. N. Zeng, J. Chen, R. G. Lin, W. E. Zhuang, R. Cao and Z. J. Lin, *Inorg. Chem.*, 2019, **58**, 6983–6992.
26 L. Feng, Y. Wang, S. Yuan, K. Y. Wang, J. L. Li, G. S. Day, D. Qiu, L. Cheng, W. M. Chen, S. T. Madrahimov and H. C. Zhou, *ACS Catal.*, 2019, **9**, 5111–5118.
27 K. Chattopadhyay, M. Mandal and D. K. Maiti, *ACS Appl. Bio Mater.*, 2021, **4**, 8159–8171.
28 S. Bazzazan, K. Moeinabadi-Bidgoli, Z. A. Lalami, S. Bazzazan, M. Mehrarya, F. E. Yeganeh, F. Hejabi, I. Akbarzadeh, H. Noorbazargan, M. Jahanbakhshi and N. Hossein-khannazer, *J. Drug Delivery Sci. Technol.*, 2023, **79**, 104009.
29 M. Pourmadadi, M. M. Eshaghi, S. Ostovar, A. Shamsabadipour, S. Safakhah, M. S. Mousavi, A. Rahdar and S. Pandey, *J. Drug Delivery Sci. Technol.*, 2022, 103758.
30 M. Pourmadadi, Z. Omrani, Z. Forootan, M. S. Ebadi and F. Yazdian, *J. Drug Delivery Sci. Technol.*, 2023, 104690.
31 H. N. Abdelhamid, *Dalton Trans.*, 2020, **49**, 10851–10857.
32 Y. Zhao, M. Zhu, H. Shang, Y. Cheng, D. Ramella, K. Zhu and Y. Luan, *New J. Chem.*, 2022, **46**, 3199–3206.
33 C. Wang, H. Zhang, Y. Wang, J. Wu, K. O. Kirlikovali, P. Li, Y. Zhou and O. K. Farha, *Small*, 2023, **19**, 2206116.
34 X. Guo, N. Zhu, Y. Lou, S. Ren, S. Pang, Y. He, X. B. Chen, Z. Shi and S. Feng, *Chem. Commun.*, 2020, **56**, 5389–5392.
35 M. Shao, Y. Li, M. Chen, W. Liu, Y. Sun, Y. Chu, Y. Sun, X. Li, R. Zhang and L. Zhang, *ChemElectroChem*, 2022, **9**, e202200866.
36 T. K. Vo, V. N. Le, K. S. Yoo, M. Song, D. Kim and J. Kim, *Cryst. Growth Des.*, 2019, **19**, 4949–4956.
37 S. Carrasco, A. Sanz-Marco and B. Martín-Matute, *Organometallics*, 2019, **38**, 3429–3435.
38 L. González, R. Gil-San-Millán, J. A. Navarro, C. R. Maldonado, E. Barea and F. J. Carmona, *J. Mater. Chem. A*, 2022, **10**, 19606–19611.
39 A. R. P. Hidayat, L. L. Zulfa, A. R. Widyanto, R. Abdullah, Y. Kusumawati and R. Ediati, *RSC Adv.*, 2023, **13**, 12320–12343.
40 K. Yu, Y. R. Lee, J. Y. Seo, K. Y. Baek, Y. M. Chung and W. S. Ahn, *Microporous Mesoporous Mater.*, 2021, **316**, 110985.
41 T. Zhang, J. Z. Wei, X. J. Sun, X. J. Zhao, H. L. Tang, H. Yan and F. M. Zhang, *Inorg. Chem.*, 2020, **59**, 8827–8835.
42 T. Zhang, J. Z. Wei, X. J. Sun, X. J. Zhao, H. L. Tang, H. Yan and F. M. Zhang, *Inorg. Chem. Commun.*, 2020, **111**, 107671.
43 A. M. Fidelli, B. Karadeniz, A. J. Howarth, I. Huskić, L. S. Germann, I. Halasz, M. Etter, S. Y. Moon, R. E. Dinnebier, V. Stilinović and O. K. Farha, *Chem. Commun.*, 2018, **54**, 6999–7002.
44 B. Karadeniz, D. Žilić, I. Huskić, L. S. Germann, A. M. Fidelli, S. Muratović, I. Lončarić, M. Etter, R. E. Dinnebier, D. Barišić and N. Cindro, *J. Am. Chem. Soc.*, 2019, **141**, 19214–19220.
45 C. He, K. Lu, D. Liu and W. Lin, *J. Am. Chem. Soc.*, 2014, **136**, 5181–5184.
46 Z. Xu, Z. Wu, S. Huang, K. Ye, Y. Jiang, J. Liu, J. Liu, X. Lu and B. Li, *J. Controlled Releasee*, 2023, **354**, 615–625.
47 J. Hu, Z. Xu, D. Liao, Y. Jiang, H. Pu, Z. Wu, X. Xu, Z. Zhao, J. Liu, X. Lu and X. Liu, *Adv. Healthcare Mater.*, 2023, 2301316.
48 H. Lv, Y. Zhang, P. Chen, J. Xue, X. Jia and J. Chen, *Langmuir*, 2020, **36**, 4025–4032.
49 H. Chen, Y. Fu, K. Feng, Y. Zhou, X. Wang, H. Huang, Y. Chen, W. Wang, Y. Xu, H. Tian and Y. Mao, *J. Nanobiotechnol.*, 2021, **19**, 1–18.
50 A. A. Hassabo, A. M. Mousa, H. Abdel-Gawad, M. H. Selim and R. M. Abdelhameed, *J. Mater. Chem. B*, 2019, **7**, 3268–3278.
51 D. Chen, J. Bi, J. Wu and A. Kumar, *J. Inorg. Organomet. Polym. Mater.*, 2020, **30**, 573–579.
52 W. Liu, Y. Pan, Y. Zhong, B. Li, Q. Ding, H. Xu, Y. Qiu, F. Ren, B. Li, M. Muddassir and J. Liu, *Chem. Eng. J.*, 2021, **412**, 127899.
53 Z. Deng, C. Fang, X. Ma, X. Li, Y. J. Zeng and X. Peng, *ACS Appl. Mater. Interfaces*, 2020, **12**, 20321–20330.
54 G. Y. Zhang, Y. H. Zhuang, D. Shan, G. F. Su, S. Cosnier and X. J. Zhang, *Anal. Chem.*, 2016, **88**, 11207–11212.

55 G. Zhang, D. Shan, H. Dong, S. Cosnier, K. A. Al-Ghanim, Z. Ahmad, S. Mahboob and X. Zhang, *Anal. Chem.*, 2018, **90**, 12284–12291.
56 L. Wu, Y. Luo, C. Wang, S. Wu, Y. Zheng, Z. Li, Z. Cui, Y. Liang, S. Zhu, J. Shen and X. Liu, *ACS Nano*, 2023, **17**, 1448–1463.
57 P. J. Jodłowski, K. Dymek, G. Kurowski, J. Jaśkowska, W. Bury, M. Pander, S. Wnorowska, K. Targowska-Duda, W. Piskorz, A. Wnorowski and A. Boguszewska-Czubara, *ACS Appl. Mater. Interfaces*, 2022, **14**, 28615–28627.
58 J. Gandara-Loe, I. Ortuño-Lizarán, L. Fernández-Sanchez, J. L. Alió, N. Cuenca, A. Vega-Estrada and J. Silvestre-Albero, *ACS Appl. Mater. Interfaces*, 2018, **11**, 1924–1931.
59 Y. Li, Z. Di, J. Gao, P. Cheng, C. Di, G. Zhang, B. Liu, X. Shi, L. D. Sun, L. Li and C. H. Yan, *J. Am. Chem. Soc.*, 2017, **139**, 13804–13810.
60 L. He, M. Brasino, C. Mao, S. Cho, W. Park, A. P. Goodwin and J. N. Cha, *Small*, 2017, **13**, 1700504.
61 W. Ning, Z. Di, Y. Yu, P. Zeng, C. Di, D. Chen, X. Kong, G. Nie, Y. Zhao and L. Li, *Small*, 2018, **14**, 1703812.
62 J. Park, Q. Jiang, D. Feng, L. Mao and H. C. Zhou, *J. Am. Chem. Soc.*, 2016, **138**, 3518–3525.
63 Y. Zhang, Q. Wang, G. Chen and P. Shi, *Inorg. Chem.*, 2019, **58**, 6593–6596.
64 Y. Zhang, F. Wang, C. Liu, Z. Wang, L. Kang, Y. Huang, K. Dong, J. Ren and X. Qu, *ACS Nano*, 2018, **12**, 651–661.
65 S. S. Wan, J. Y. Zeng, H. Cheng and X. Z. Zhang, *Biomater.*, 2018, **185**, 51–62.
66 D. Feng, W. C. Chung, Z. Wei, Z. Y. Gu, H. L. Jiang, Y. P. Chen, D. J. Darensbourg and H. C. Zhou, *J. Am. Chem. Soc.*, 2013, **135**, 17105–17110.
67 Z. Sun, J. Li, Y. Tong, H. Han, Y. Yang, C. Wang, H. Li, L. Du and Y. Jiang, *Anal. Chim. Acta*, 2022, **1221**, 340136.
68 T. Y. Huang, C. W. Kung, Y. T. Liao, S. Y. Kao, M. Cheng, T. H. Chang, J. Henzie, H. R. Alamri, Z. A. Alothman, Y. Yamauchi and K. C. Ho, *Adv. Sci.*, 2017, **4**, 1700261.
69 W. Duan, B. Li, W. Zhang, J. Li, X. Yao, Y. Tian, J. Zheng and D. Li, *J. Nanobiotechnol.*, 2022, **20**, 1–12.
70 H. Furukawa, F. Gándara, Y. B. Zhang, J. Jiang, W. L. Queen, M. R. Hudson and O. M. Yaghi, *J. Am. Chem. Soc.*, 2014, **136**, 4369–4381.
71 F. Demir Duman, A. Monaco, R. Foulkes, C. R. Becer and R. S. Forgan, *ACS Appl. Nano Mater.*, 2022, **5**, 13862–13873.
72 M. Parsaei and K. Akhbari, *Inorg. Chem.*, 2022, **61**, 19354–19368.
73 S. Biswas, Q. Lan, Y. Xie, X. Sun and Y. Wang, *ACS Appl. Mater. Interfaces*, 2021, **13**, 3295–3302.
74 X. Zhao, S. Liu, C. Hu, Y. Liu, M. Pang and J. Lin, *ACS Appl. Bio Mater.*, 2019, **2**, 4436–4441.
75 S. Kato, K. I. Otake, H. Chen, I. Akpinar, C. T. Buru, T. Islamoglu, R. Q. Snurr and O. K. Farha, *J. Am. Chem. Soc.*, 2019, **141**, 2568–2576.